

Recognition of Unit Disk Graphs for Caterpillars, Embedded Trees, and Outerplanar Graphs

Sujoy Bhore ✉ 

Université Libre de Bruxelles, Brussels, Belgium.

Soeren Nickel ✉ 

TU Wien, Austria.

Martin Nöllenburg ✉ 

TU Wien, Austria.

Abstract

Unit disk graphs are graphs that have a *unit disk intersection representation* (UDR). In the recognition problem the objective is to decide whether a given graph is a unit disk graph, which is known to be NP-hard, even for planar graphs. In this work, we show that the recognition of unit disk graphs remains NP-hard for outerplanar graphs and for embedded trees. We also show that given a caterpillar graph, we can decide in linear time whether it is a unit disk graph.

2012 ACM Subject Classification Theory of computation → Computational geometry

Keywords and phrases Unit disk graphs, outerplanar graphs, caterpillars, Embedded trees.

Funding *Sujoy Bhore*: Research on this paper was supported by the Fonds de la Recherche Scientifique-FNRS under Grant no MISU F 6001 and by the Austrian Science Fund (FWF) under grant P31119.

1 Introduction

The representation of graphs as contacts or intersections of unit disks has been a major topic of investigation in geometric graph theory. A set of unit disks in \mathbb{R}^2 is a unit disk intersection representation (UDR) of a graph $G = (V, E)$, if there is a bijection between V and the set of unit disks such that two disks intersect if and only if they are adjacent in G . *Unit disk graphs* are graphs that admit UDR. *Unit disk contact graphs* (also known as penny graphs) are the subfamily of unit disk graphs that have a UDR with interior-disjoint disks, also called a *unit disk contact representation* (UDC). The famous circle packing theorem states that every planar graph has a contact representation by touching disks and vice versa [14]. Since then, a large body of research has been devoted to the representation of planar graphs as a contacts or intersections of geometric objects [4, 5, 9, 10].

The recognition problem, where the objective is to decide whether a given graph admits a UDR, has a rich history [1, 2, 11, 12]. Breu and Kirpatrick [3] proved that it is NP-hard to decide whether a graph G admits a UDR or a UDC. Klemz et al. [13] showed that recognizing outerplanar unit disk contact graphs is already NP-hard, but decidable in linear time for caterpillars, i.e., trees whose internal nodes form a path. Eades and Wormald [8] showed that it is NP-hard to decide whether a given tree is a subgraph of a unit disk contact graph.

Recognition with a fixed embedding is an important variant of the recognition problem. Given a plane graph G , the objective in this problem is to decide whether G is a contact graph of interior-disjoint unit disks in the plane with the same cyclic order of neighbors at each vertex. Some recent works investigated the recognition problem of UDC with/without fixed embedding, and narrowed down the precise boundary between hardness and tractability; see [1, 6, 7].

Most of the existing hardness results either rely on graphs with a large number of cycles, as also noted by Bowen et al. [1], or uses the fixed embedding to enforce certain

representations [1, 6]. Therefore, an important open question in this area is to show the complexity of the recognition problem for non-embedded trees.

Our Contribution. We show that recognizing unit disk graphs is NP-hard for outerplanar graphs and for embedded trees (Section 3), but decidable in linear time for caterpillars (Section 4).

2 Preliminaries

A graph $G = (V, E)$ with $V = \{v_1, \dots, v_n\}$ is a unit disk graph if there exists a set of closed unit disks $\mathcal{D} = \{d_1, \dots, d_n\}$ and a bijective mapping $d: V \rightarrow \mathcal{D}$, s.t., $d(v_i) = d_i$ and $v_i v_j \in E$ if and only if d_i and d_j intersect. We call \mathcal{D} a *unit disk intersection representation* (UDR) of G . If all disks in \mathcal{D} are pairwise interior disjoint we speak of a *unit disk contact representation* (UDC) of G . A graph is a *unit disk contact graph* if it admits a UDC.

The set of disks \mathcal{D} induces an embedding of G by placing every vertex v at the center of $d(v)$ and linking neighboring vertices by straight-line edges. We will therefore also use v as the center of $d(v)$. We use $\mathcal{E}_{\mathcal{D}}(G)$ for the embedding induced by \mathcal{D} . We say a UDR \mathcal{D} preserves the embedding of an embedded graph G with embedding $\mathcal{E}(G)$ if $\mathcal{E}_{\mathcal{D}}(G) = \mathcal{E}(G)$. The notation $\angle abc$ indicated the clockwise angle between ab and bc . We define the angle $\angle d_i d_j d_k$ as the clockwise angle $\angle v_i v_j v_k$ in $\mathcal{E}_{\mathcal{D}}(G)$.

3 Hardness Results

Bowen et al. [1] proved that recognizing unit disk contact graphs is NP-hard for embedded trees, via a reduction from planar 3-SAT, which uses an auxiliary construction formulated as a realization of a polygonal linkage. Polygonal linkages are explained in Section 3.1. The details of this auxiliary structure are explained in Section 3.2. Then a tree, whose UDC is an approximation of the auxiliary structure and which mimics the shape and behaviour of it, is constructed. This construction is summarized in Section 3.3.

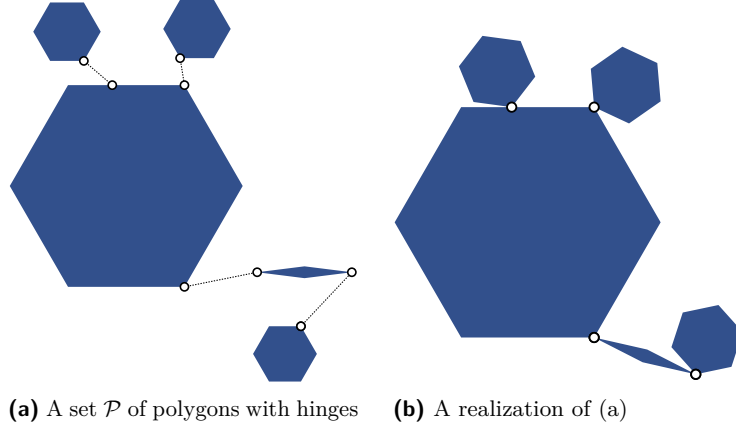
After this recapitulation of the results of Bowen et al. [1], we adapt this result to prove that recognizing unit disk graphs is NP-hard for outerplanar graphs (Section 3.4) and trees with a fixed embedding (Section 3.5).

3.1 Polygonal Linkages

Bowen et al. [1] considered multiple problems in their work, one of which is the *polygonal linkage realizability* (PLR) problem. A polygonal linkage is a set \mathcal{P} of convex polygons and a set H of hinges. One hinge is a set of two or more points on the boundaries of distinct polygons. A polygonal linkage is realizable, if every $p \in \mathcal{P}$ can be placed in the plane, s.t.

- all polygons are interior disjoint
- for every hinge $h \in H$, all points of the hinge coincide and
- a predefined cyclic order of adjacent polygons around every hinge is kept.

In our case and in the case of this reduction, hinges are only of size two, i.e., a realization will identify exactly two points on distinct polygons per hinge. This means that cyclic order around hinges is always kept by default. A polygonal linkage and its realization are shown in Figure 1.



■ **Figure 1** An instance of PLR (a), where points belonging to the same hinge are indicated with a dotted line connection. A placement of (rotated and/or translated) copies of the polygons in \mathcal{P} in the plane is a realization (b) if the points of the same hinge are identified.

3.2 Auxiliary Structure

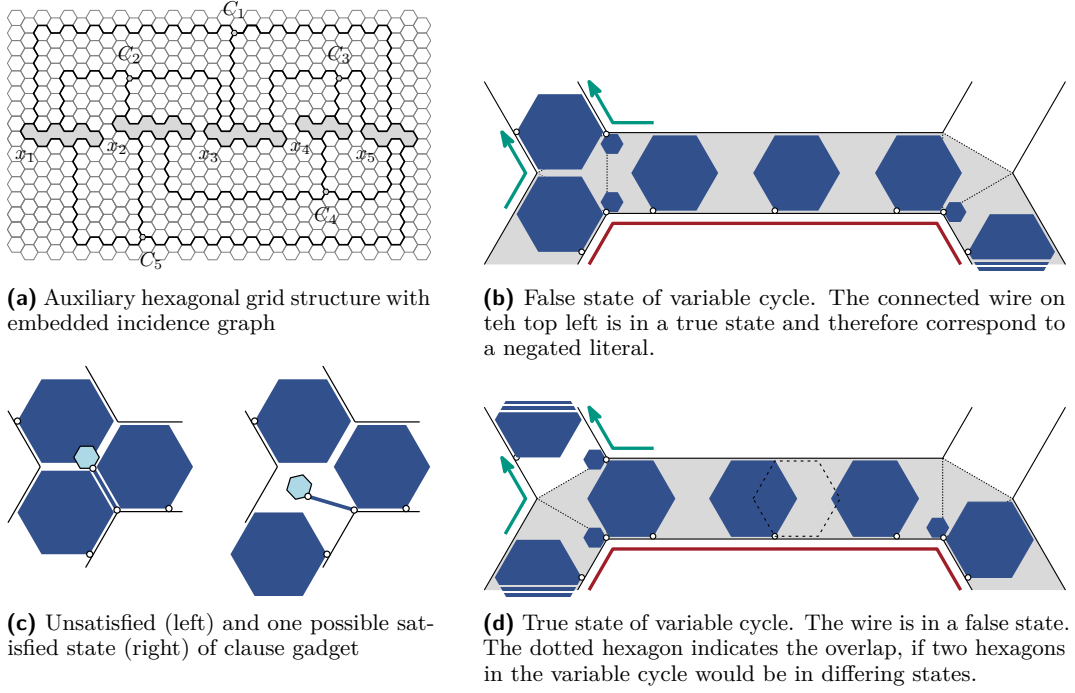
The auxiliary structure mimics a hexagonal grid. This grid-like structure is obtained by using a hexagonal tiling of the plane and then shrinking every hexagon by a small amount to obtain narrow channels of a fixed height between two hexagons, where ε is a sufficiently small constant. At the corners of the hexagons, three such channels meet to form a junction. The union of all channels and junctions forms the grid-like structure. In this grid, a representation of the incidence graph G_ϕ of the planar 3-SAT instance ϕ is fitted, see Figure 2a.

A variable v of ϕ is represented in this grid as an alternating cycle of channels and junctions, indicated with a grey fill in Figure 2a. In such a cycle the channels can be filled with smaller hexagons of height h , which are connected to the large hexagon on the side of the channel – which is on the “inside” of the variable cycle – via a junction. In a channel, one corner of each of the small hexagons is connected to the large hexagon via a hinge, s.t., the small hexagon can be “flipped” around this junction. Due to the chosen size, the hexagon can be realized in one of two states, see Figures 2b and 2d. The distance of the hinges of neighboring small hexagons is chosen in such a way that the state of one hexagon determines the state of all hexagons in the channel, see Figure 2d. At each junction, we add an even smaller hexagon with a hinge to the corner of that large hexagon, which is adjacent to the channels on either side of the junction in the variable cycle. This propagates the state of the hexagons in one channel through the junction into the other channel and so throughout the entire cycle. See Figures 2b and 2d for a detailed explanation.

Wire gadgets are alternating paths of channels and junctions, which use the same mechanism to propagate the state of the hexagons in the channels and therefore admit two states overall.

Wire gadgets can be connected to a variable cycle at every junction using the third unoccupied channel and adding a second very small hexagon in the junction. A wire gadget is considered to transmit the value *true*, if and only if, part of the first small hexagon of the first channel of the wire gadget enters into the junction. By placing the small hexagon on one or the other corner (cf. Figures 2b and 2d) the truth value which is transmitted can be “inverted” if necessary.

For every clause in ϕ , three such wire gadgets are connected to the variable cycles of the occurring variables and the wires are routed to meet in a junction. This junction contains a



■ **Figure 2** Auxiliary structure details used by Bowen et al. [1]. All Figures are recreations from their paper. The incidence graph is embedded on a hexagonal grid (a). The edges are short corridors in which the blue hexagons are fitted, hinged at white vertices. Hexagons in the variable cycle (red line, grey backdrop) have two states (b) and (d). The clause gadget (c) requires one hexagon, which does not enter the junction.

small hexagon connected to the corner of a large hexagon via a long and very thin rhombus (in place of a line segment), s.t., an overlap-free realization is only possible, if at least one connected wire gadget has no hexagon entering the junction and is therefore in a true state, see Figure 2c.

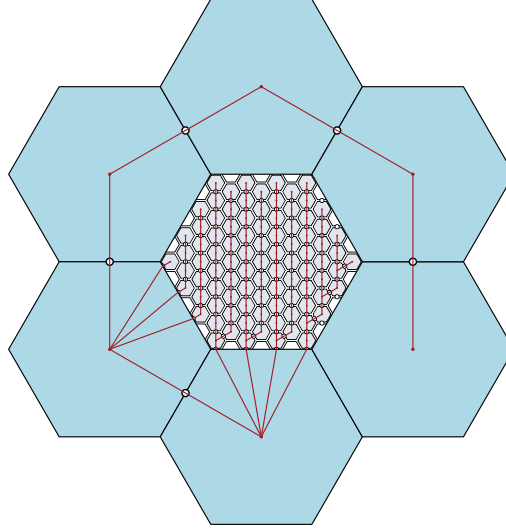
In order to guarantee a somewhat rigid placement of these hexagons, the entire construction is surrounded by a set of six huge hexagons, and the hexagons acting as the faces of the hexagonal grid are column-wise connected (cf. Figure 3). This restricts the position of the large hexagons to an N -neighborhood, where N is a polynomial of the number of variables and clauses in ϕ [1].

Note that the connections between the polygons in the polygonal linkage induce a tree. In particular note that we can replace the hexagons with outerplanar graphs and replace the hinges between them with paths of length one to three and the entire construction remains an outerplanar graph. The same way we can replace all hexagons with trees and replace the hinges with vertex paths of length one to three and the entire construction remains a tree.

For a more detailed description, a full construction and the proof of the semi-rigid placement we refer to the original paper of Bowen et al. [1].

3.3 Approximating the Auxilliary Structure

In order to prove the NP-hardness for recognition of unit disk contact graphs, Bowen et al. [1] created λ -stable approximations of the basic building blocks of the auxilliary structure (hexagons of varying sizes and long thin rhombi). A graph is a λ -stable approximation of



■ **Figure 3** The composition of the rigid structure as a realization of a polygonal linkage. Hinges are indicated by points. The figure is a recreation of a similar figure in [1], augmented with lines, which emphasize the tree-like structure of connections in the polygonal linkage.

a polygon P , if the boundary union of all disks in its UDC is necessarily within a constant Hausdorff distance λ of a congruent copy of P .

Bowen et al. described the construction procedures for two graphs T_k, T'_k , which are 2-stable approximations of a long thin rhombus and a regular hexagon. These two graphs are shown in Figure 4. For the details of these constructions, we again refer to Bowen et al. [1]. The construction of our building blocks using outerplanar graphs in Section 3.4 and embedded trees Section 3.5 is based on these graphs.

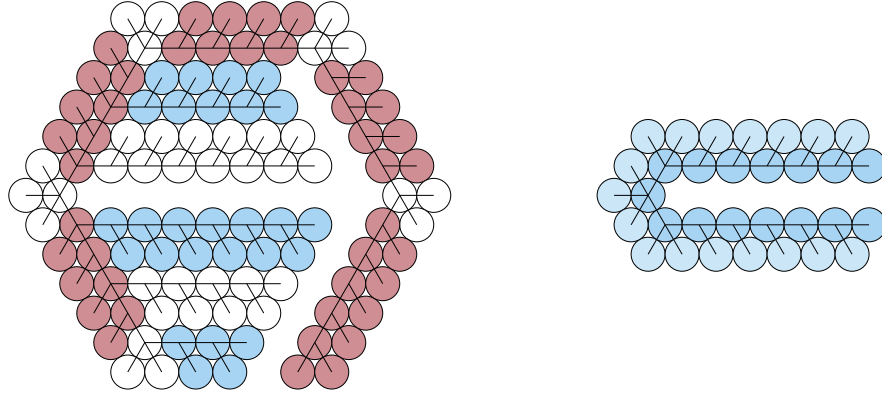
It remains to discuss how the hinges are modeled. Two λ -stable approximations G, G' of two polygons P, P' are connected with a path of vertices of constant length, if there exists a hinge $h \in H$, with one point on the boundary of P and the other on the boundary of P' . The exact length of the path is dependent on the location of the hinge. If the hinge is not placed on a corner of either polygon, they are simply connected via a single cut vertex, and with a path of length three otherwise, in order to facilitate more movement, which mimics the possibility of polygons to rotate around hinges. The union of the UDC of two thus connected graphs G, G' , remains a constant factor approximation of a congruent copy of the realization of $P \cup P'$.

3.4 Outerplanar Graphs

► **Theorem 3.1.** *Recognizing unit disk graphs is NP-hard for outerplanar graphs.*

To prove this theorem, we first extend the notion of λ -stable approximations [1] to UDRs.

► **Definition 3.2.** *A graph G is a λ -stable approximation of a polygonal shape P if, in every UDR of G , a congruent copy of P and the union of all unit disks in the UDR have at most a Hausdorff distance of λ .*

(a) Graph T_k and its UDC(b) Graph T'_k and its UDC

■ **Figure 4** The 2-stable approximations of a long thin rhombus (a) and a regular hexagon (b). All Figures are recreations from Bowen et al. [1].

We will provide outerplanar graphs G_k^H and G_k^R , which are $O(1)$ -stable approximations of a hexagon and a rhombus, respectively. Then the NP-hardness follows immediately from the construction of Bowen et al. [1] sketched above.

First a ladder L_k consists of two paths v_1, v_2, \dots, v_k and v'_1, v'_2, \dots, v'_k of vertices – also called the *outer* and *inner* vertices respectively – s.t., each pair (v_i, v'_i) is connected with an edge. The blue vertices in Figure 5a form a ladder, specifically L_{17} . A UDR of L_{17} is shown in the blue disks of Figure 5c.

► **Lemma 3.3.** *Let $k \in \mathbb{N}$ and let \mathcal{D} be a UDR of L_k . Then $\mathcal{E}_{\mathcal{D}}(L_k)$ induces the same embedding as shown in Figure 5a, which is outerplanar.*

Proof. Clearly no disk can be placed inside a UDR of a C_4 , without intersecting at least two disks of the C_4 . Since every disk $d(v_i)$ of a vertex v_i , which is not part of the C_4 intersects at most one disk of the C_4 , this is impossible and the outer face is fixed. Therefore the induced embedding is unique. ◀

Lemma 3.3 implies that we can assign a clear “outer side”, i.e., $d(v_1), \dots, d(v_k)$ and “inner side”, i.e., $d(v'_1), \dots, d(v'_k)$ to a UDR of L_k .

Next we want to ensure that any overall bend towards the outer side is impossible. For this we will augment L_k with additional neighbors. We restrict the ladders to an odd length and alternatingly add one and two leaf neighbors, which we will call extension neighbors. The resulting graph can be seen in Figure 5a.

► **Lemma 3.4.** *Let $(v_1, v_2, v_3, v_4, v_5)$ be a chain of vertices on the outer side of a ladder L_k with one, two, one, two and one extension neighbor respectively. Then the sum of angles $\gamma = \angle v_3 v_2 v_1 + \angle v_4 v_3 v_2 + \angle v_5 v_4 v_3$ in a UDR of L_k is smaller than 3π , i.e., overall we bend more towards the inner side than towards the outer side.*

Proof. We will refer to the two extension neighbors of v_2 as a and a' , both of which are placed on the outer side of the ladder. Similar we will call the extension neighbors of v_4 , b and b' . The singular extension neighbor of v_3 , will be referred to as c . The naming is also shown in Figure 6a. Without loss of generality, we assume that the clockwise order on v_2 is

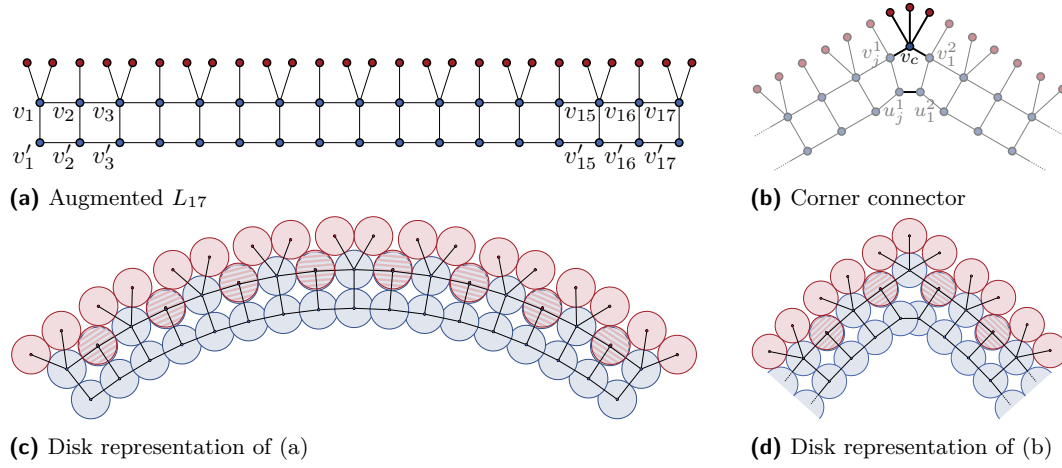


Figure 5 The components used to create the λ -stable approximations G_k^H and G_k^R Graph L_{17} . A ladder of length 17 (a) and its UDR (c), as well as a corner connector (b) and its UDR (d). The corner connector is connected to two ladders of length j (lighter colored parts) and the actual parts of the corner connector are colored in a darker color in (b). The bends in the UDRs are required but exaggerated.

(v_1, a, a', v_3, v'_2) and analogue the clockwise order on v_4 is (v_3, b, b', v_5, v'_4) . Figures 6a and 6c depict this placement and its UDR.

First observe that $\angle v_1 v_2 a > \frac{\pi}{3}$, since $|v_1 v_2| \leq 2$, $|v_2 a| \leq 2$ and $|v_1 a| > 2$. For the same reason we have $\angle a v_2 a' > \frac{\pi}{3}$ and $\angle a' v_2 v_3 > \frac{\pi}{3}$. This means that

$$\angle v_1 v_2 v_3 = \angle v_1 v_2 a + \angle a v_2 a' + \angle a' v_2 v_3 > \pi$$

and similarly $\angle v_3 v_4 v_5 > \pi$.

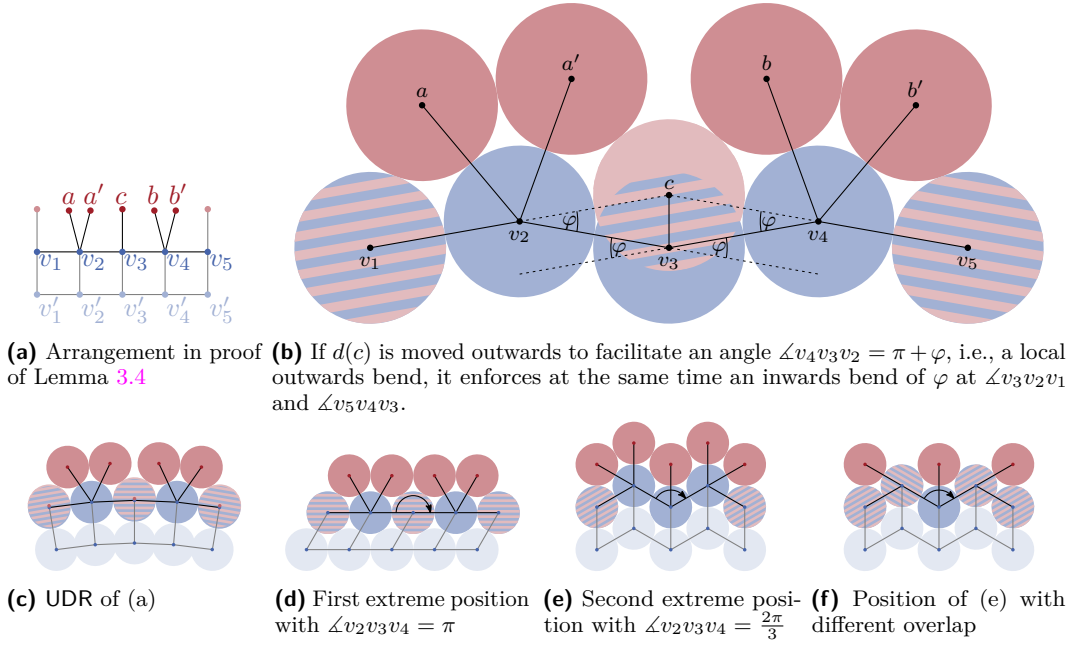
Now we will distinguish two extremes at v_3 . In the first extreme position $d(c)$ is placed almost on top of $d(v_3)$, s.t., $\angle v_2 v_3 c = \angle c v_3 v_4 = \alpha$ and α tends toward $\frac{\pi}{2}$ as $|v_3 c|$ approaches 0. The extreme placement with $|v_3 c|$ equal to 0 is shown in Figure 6d. This results in $\angle v_2 v_3 v_4 > \pi$. To reach the second extreme (cf. Figure 6e) $d(c)$ is moved outwards. As $|v_3 c|$ increases, it facilitates a local outward bend and an angle $\angle v_2 v_3 v_4 > \pi - \varphi$, where $\varphi = \cos^{-1} \left(\frac{|v_2 c|^2 + |v_2 v_3|^2 - |v_3 c|^2}{2|v_2 c||v_2 v_3|} \right)$, see Figure 6b. However, in order to maximize this bend, v_2 and v_4 are moved into the resulting gap between v_3 and c , s.t., the distances $|v_2 c|$ and $|v_4 c|$ are equal to $2 + \varepsilon'$, where ε' is a very small constant. In particular we have $\angle a' v_2 c > \frac{\pi}{3}$, and similarly $\angle c v_4 b > \frac{\pi}{3}$. Finally this leads to the following values:

$$\begin{aligned} \angle v_1 v_2 v_3 &= \angle v_1 v_2 a + \angle a v_2 a' + \angle a' v_2 c + \angle c v_2 v_3 \geq \frac{\pi}{3} + \frac{\pi}{3} + \frac{\pi}{3} + \varphi = \pi + \varphi \\ \angle v_3 v_4 v_5 &= \angle v_3 v_4 c + \angle c v_4 b + \angle b v_4 b' + \angle b' v_4 v_5 \geq \varphi + \frac{\pi}{3} + \frac{\pi}{3} + \frac{\pi}{3} = \pi + \varphi \end{aligned}$$

Clearly the overall bend towards the inside is minimized, if φ and therefore $|v_3 c|$ is minimal, i.e., we are as close as possible to the first extreme state. Since $|v_3 c| > 0$, we have $\angle v_2 v_3 v_4 > \pi$ and finally

$$\gamma = \angle v_1 v_2 v_3 + \angle v_2 v_3 v_4 + \angle v_3 v_4 v_5 > 3\pi$$

Note that the second extreme position can also be achieved by using more overlap between $d(v_2)$ or $d(v_4)$ and one of their extension neighbors, however, this configuration forces $\angle a v_2 v_3$



■ **Figure 6** Figures for proof of Lemma 3.4.

and $\angle v_3v_4b'$ to approach π and therefore results in a similar overall inwards bend by φ , as shown in Figure 6f.

We can also add a third extension neighbor to an outer vertex of a ladder to force an even more pronounced bend towards the inside. The corresponding graph construction is shown in Figure 5b and a valid UDR in Figure 5d.

► **Lemma 3.5.** *Let (v_1, v_2, v_3) be a chain of outside vertices of a ladder, s.t., v_2 has degree 5, i.e., 3 extension neighbors. Then the angle $\angle v_3v_2v_1$ is smaller than $\frac{2\pi}{3}$, i.e., overall we bend at least 60° towards the inner side.*

Proof. Note that the argument for the inward directed bend at v_2 and v_4 in the proof of Lemma 3.4 was simply based on the number of extension neighbors. By increasing that number to 3, the lemma immediately follows.

We call this construction a corner connector. The corner connector contains a 5-cycle, however similar to a 4-cycle, it is impossible to place a disk inside such a cycle without creating wrong adjacencies through overlap.

Finally we want to state some measure for the height of a UDR of an augmented L_k

► **Lemma 3.6.** *The height the smallest bounding rectangle of a UDR of an augmented ladder L_k is at least $2\sqrt{3} + 2 - \varepsilon''$, where ε'' is a very small constant, which is the height of the smallest bounding box of an optimal packing of three rows of unit disks minus ε'' .*

Proof. The distance between the extension neighbors and the outer disks of the ladder has been argued in the proof of Lemma 3.4. Recall that the disks of the outside vertices of the ladder with a single extension neighbor are almost completely covered by it. Let $d(v_k)$ be such a covered disk. Its adjacent disk $d(v'_k)$ on the inside of the ladder can therefore only

overlap a very small amount with $d(v_k)$. Since $d(v'_k)$ is disjoint from $d(v_{k-1})$ and $d(v_{k+1})$, the extreme position (see Figure 6d) results in the smallest overall height of the ladder, which is the height of the dense packing of three rows of unit disks, i.e., $2\sqrt{3} + 2$ minus the small amount ε'' which is attributed to the small possible overlap of $d(v'_k)$ and $d(v_k)$. ◀

Now we have all necessities to describe the construction of the $O(1)$ -stable approximations of a long thin rhombus (Lemma 3.7) and a regular hexagon (Lemma 3.8).

Two ladders L_k and L'_k are placed opposite each other and connected on one end with three corner connectors as shown in Figure 7. Note that the horizontal distance between c_0 and v_1 is four. The following lemma is analogue to Lemma 10 in [1].

► **Lemma 3.7.** *For every integer k the outerplanar graph G_k^R in Figure 7 is a 7-stable approximation of a rhombus of width $2k + 6$ and height $6\sqrt{3} + 2$.*

Proof. We can assume that $v_0 = (0, 0)$ and that $c_0 = (-2, 0)$. We define a point $l_0 = (2k+4, 0)$ on the positive x -axis with.

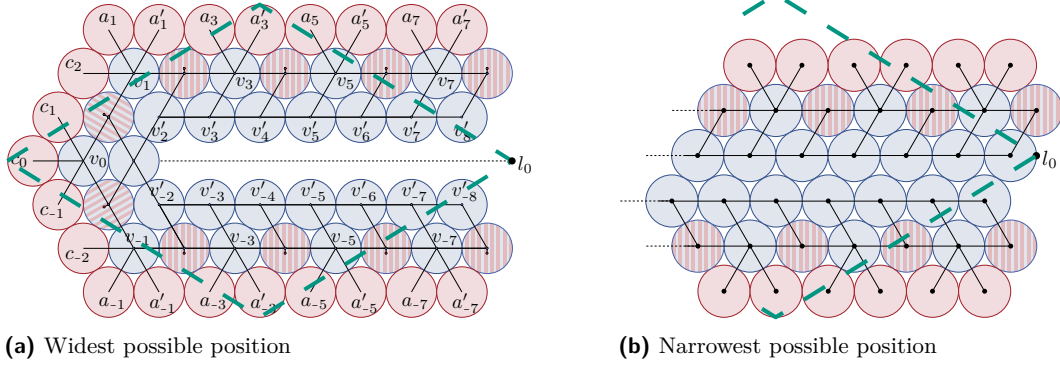
We place a congruent copy of the rhombus, s.t., the long diagonal aligns with $\{c_0 l_0\}$, and one corner point coincides with the leftmost point of c_0 , which is at $(-3, 0)$. At every point the upper and lower boundary of the rhombus has a vertical distance of $\delta \in [0, 3\sqrt{3} + 1]$ to $c_0 l_0$. Due to Lemmata 3.4 and 3.5, the overall bend of L_k and L'_k has to be towards the inner side. In fact the position depicted in the Figure 7a is the limit and would require an additional infinitesimal bend inwards to be valid. A consequence is that c_0 and any a_i , have a maximal vertical distance of $3\sqrt{3}$ and therefore any point on the boundary of any disk has at most a vertical distance of $3\sqrt{3} + 1 \approx 6.196 < 7$ to $c_0 l_0$.

Clearly the UDRs of L_k and L'_k are completely overlap-free and therefore a tight packing as indicated in Figure 7b is the narrowest possible configuration (including a small gap between the ladders).

Now consider, that the smallest rectangular bounding box of the disks of the of outer vertices v_1, \dots, v_k and v_{-1}, \dots, v_{-k} (as labeled in Figure 7a) and their extension neighbors have a combined height of at least $3\sqrt{3} + 2$, which is the height of an optimal packing of four rows of unit disks. Therefore, at every point, there is part of the outline of G_k^R on or above, and on or below $c_0 l_0$ and the distance of the boundary of the union of all disks and the boundary of the rhombus is at most the distance of the rhombus itself to $c_0 l_0$, which as stated before, is $3\sqrt{3} + 1 < 7$. ◀

Next we will create a 5-stable approximation G_k^H of a regular hexagon by tracing the outline of a hexagon with ladders and corner connectors as shown with the blue and the red disks in Figure 8a. Every side of the hexagon is represented by a L_{k-3} . Let L_j^1, L_j^2 be two ladders, and let v_i^k and u_i^k be the i -th outer and inner vertices of L_j^k respectively. At a corner, where L_j^1 and L_j^2 meet, we connect u_j^1 and u_j^2 with an edge. Further, we connect the vertex v_c of the corner connector with v_j^1 and v_j^2 , thereby connecting the two ladders with a corner connector. The construction is depicted in Figure 5b. Six ladders are connected in this fashion through the use of five corner connectors, leaving the first and the last ladder disconnected. This forms the outer hull of the hexagon, shown in Figure 8a.

Since bends towards the outer side are impossible, we next need to control the possible deformation of a UDR of our construction towards the inner side. To achieve this, we add ladders to our construction on the inside of the hull, reminiscent of our construction of G_k^R . We chose the size of the hexagon, s.t., the inner area of a UDR of the hull admits the placement of $2m$ ladders ($m \in \mathbb{N}$ on the top and on the bottom, each) and that in a UDR, which is an optimal packing of disks, there is no space to add further disks in the gaps, without creating false adjacencies.



■ **Figure 7** A 7-stable approximation G_7^R of a rhombus superimposed on its UDR in its widest (a) and narrowest (b) configuration. Both UDRs require a small inward bend to be valid and hatched disks indicate almost overlapping placement of a red disk on a blue disk, with a small shift to the outer side. Both inward bends and outward shifts are omitted.

► **Lemma 3.8.** *For every integer $k = 6n + 4, n \in \mathbb{N}$, the outerplanar graph G_k^H in Figure 8a is a 5-stable approximation of a regular hexagon of side length $2k - 1$.*

Proof. By combining Lemmas 3.4 and 3.5, we conclude that a UDR of a such constructed outer hull does not exceed the boundary of a translated and/or rotated copy of the hexagon outlined as a dashed line in Figure 8a, which has a side length of $2k - 1$.

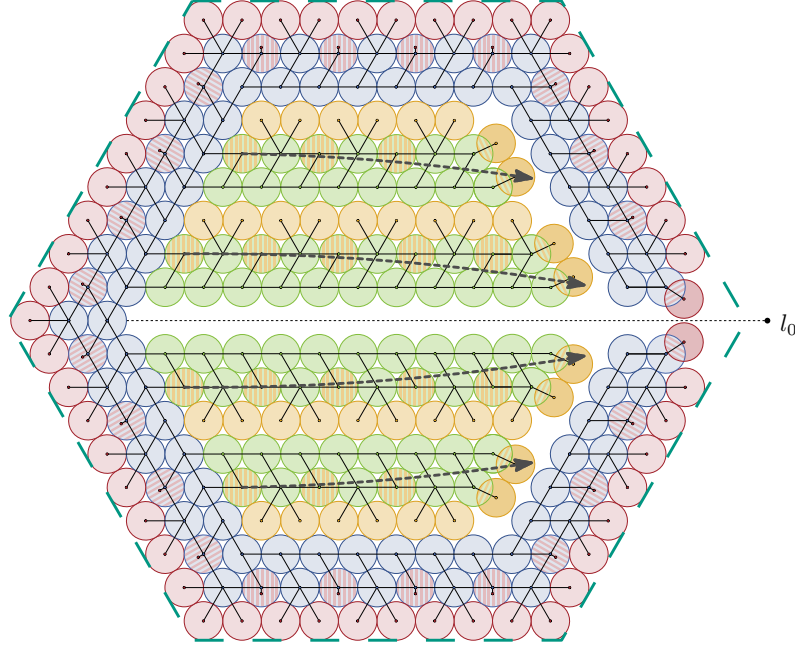
Some movement towards the inside is possible. By moving all ladders on the inside in the top half down by a complete row, including the ladder tracing the upper horizontal edge of the hexagon, we again arrive at an optimal packing of pairwise disjoint ladders, which contribute at least their full height of $2\sqrt{3} + 2 - \varepsilon''$ (again ε'' is a very small constant value) to the height of any UDR of the construction and theoretically, there is space to fold the right outer arm inward as depicted in 8b. Even though the depicted folding of this outer arm into the optimal packing position is not possible, due to the construction, for increasingly long outer arms, we can get arbitrarily close to this packing. Therefore we analyze the (unreachable) worst case of the optimal packing, in which the farthest point from the boundary of the hexagon has a distance of $2\sqrt{3} + 1 + O(k) \cdot \varepsilon''$. Since we can chose ε small enough and $2\sqrt{3} + 1 \approx 4.464 < 5$, we conclude that no point on the boundary of the union of all disks in the UDR of a G_k^H has a larger distance than 5 to a point on the boundary of the green dashed hexagon. ◀

As the last point, we emphasize that we can emulate hinges the exact same way as done in the reduction of Bowen et al. [1], and the correctness of Theorem 3.1 follows.

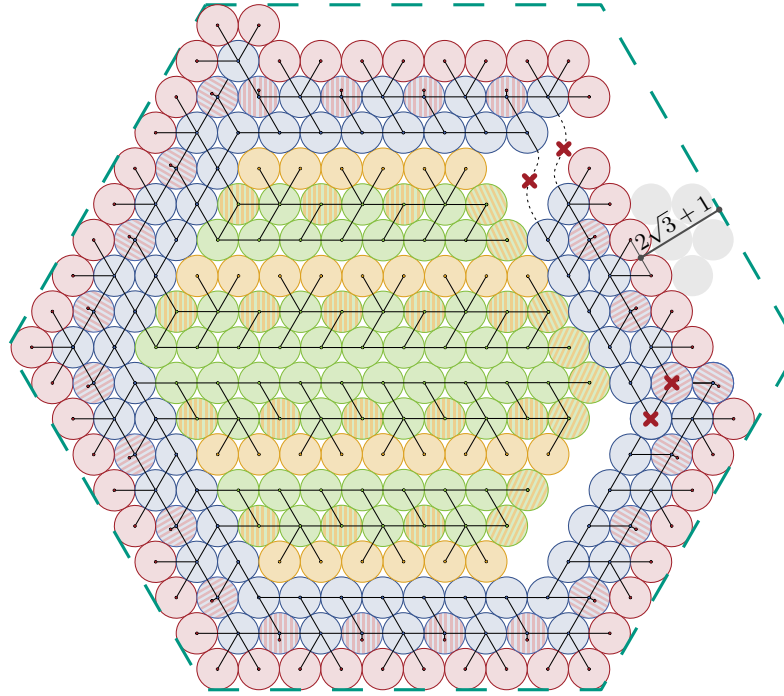
3.5 Trees with Embeddings

By slightly adapting the construction of the previous section, we can prove that given a tree T and an embedding $\mathcal{E}(T)$ it is NP-hard to decide if T admits a UDR \mathcal{D} , s.t., $\mathcal{E}_{\mathcal{D}}(T) = \mathcal{E}(T)$. In particular, we construct two graphs T_k^R, T_k^H , which are both trees and $O(1)$ -stable approximations of a long thin rhombus and a regular hexagon respectively.

In the previous proof, we needed to construct ladders in a very specific way to force the placement of the disks of extension neighbors to one side. This was done by adding the inner vertices, which made the graphs outerplanar. Since in this setting the embedding is fixed, we

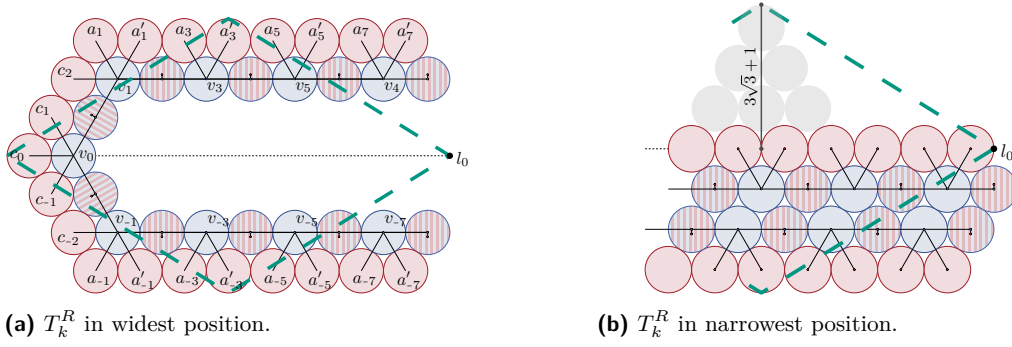


(a) Combination of the ladder and corner connectors into 5-stable approximation G_k^H of a hexagon superimposed on its UDR. Again, hatched disks indicate almost overlapping placement of disks. Necessary infinitesimal bends are omitted. The direction of these bends of the inner components is indicated with the grey arrow. The approximated regular hexagon is indicated by the dashed green outline.



(b) In the narrowest position, the UDR of a G_k^H can – similar to the rhombus – fold all inner arms to one side (here to the lower side), and theoretically, there is space to fold the outer arms inward as depicted. The UDR of the arms are however again pairwise overlap free and the largest reachable distance any point on the boundary of the union of disks can have from the approximated regular hexagon is $2\sqrt{3} + 1$. Note further that the folding of the rightmost arm is not possible as depicted, indicated by the red crossings, which mark areas of forced overlap and connections in the graph, which cannot be realized in a UDR. However in a setting with an extremely long arm, the small inward bend could lead to almost parallel arms, which run very close to each other, hence we analyze the (unreachable) worst case.

■ **Figure 8** Construction and analysis of G_k^H



■ **Figure 9** A 7-stable approximation T_k^R of a long thin rhombus superimposed on its UDR in its widest (a) and narrowest (b) possible position. In both cases at any point along c_0l_0 at least one point on the boundary of the union of all disks in a UDR of T_k^R lies on or above c_0l_0 and on or below c_0l_0 .

can remove the inner vertices, which leaves the outer vertices and the extension neighbors. Observe that the leftover graph is a tree. The same holds for the corner connector.

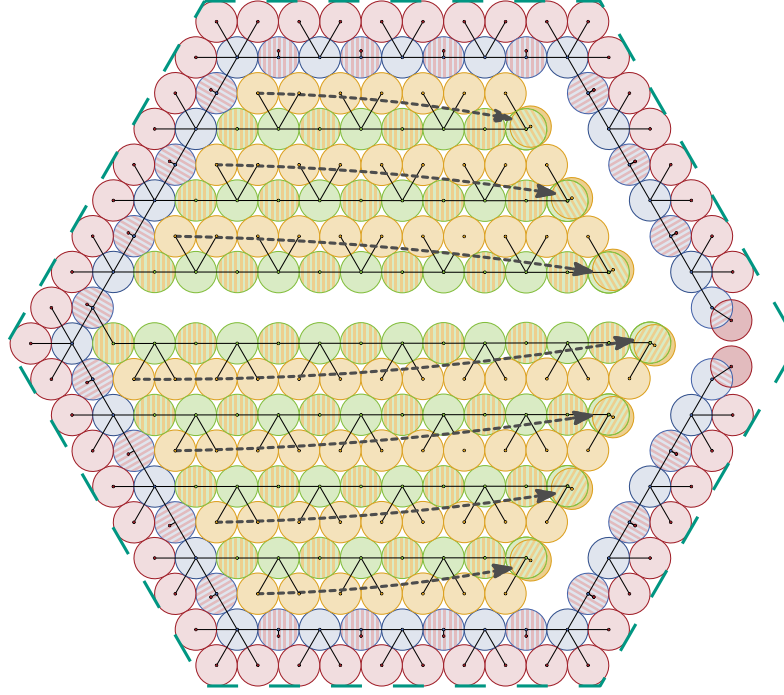
Lemma 3.4 and Lemma 3.5 can be directly applied to this new construction, since no assumption was made about the placement of the inner vertices outside of their function of forcing the disks of the extension neighbors to be placed on the outside. This is now guaranteed by the embedding that is given as input.

Next note that even without the inner vertices of the ladders, the two arms of a T_k^R must together always be at least as high as an optimal packing of four rows of disks, which results in a height of $3\sqrt{3} + 2$. Therefore, at any given horizontal point, some part of the boundary of the union of all disks in a UDR of T_k^R is either on or above c_0l_0 . Since any point on the approximated rhombus is at most $3\sqrt{3} + 1 < 7$ away from this line, T_k^R is a 7-stable approximation of a long thin rhombus.

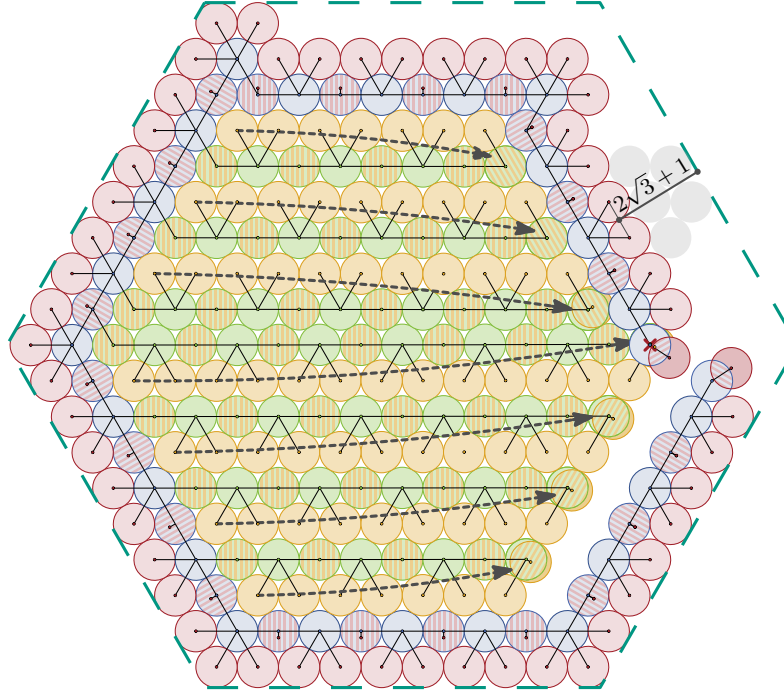
We perform a similar adaption of G_k^H to obtain T_k^H , a 5-stable approximation of a regular Hexagon. Analogously to T_k^R the outer hull, which traces the hexagon is the same as for G_k^H , with all inner vertices removed from the ladders. The relative placement of disks of extension neighbors to the outside is fixed, by the given embedding. Therefore we can always place a congruent translated and/or rotated copy of the hexagon we want to approximate over the UDR of the construction shown in Figure 10a, s.t., the UDR is completely contained.

The exact placement of the inner ladder is slightly different as before. We still fill the inside in such a manner, that the space between all upper and lower inner ladders does not admit the placement of an additional disk in a UDR, if realized as an optimal packing (cf. Figure 10a), however this requires an asymmetric construction, which places one additional ladder on one of the two sides, here to the bottom. Movement to the inside can be analyzed with a similar approach as before, by considering the closest placement to the inside of any of the arms, resulting in an optimal packing of the entire upper half of the construction, as seen in Figure 10b. Again this unobtainable worst case scenario leads to a maximal distance of $2\sqrt{3} + 1 < 5$ between the outline of any UDR of T_k^H and the hexagon.

► **Theorem 3.9.** *Recognizing unit disk graphs is NP-hard for embedded trees.*



(a) A 5-stable approximation T_k^H of a hexagon superimposed on its UDR. Note that T_k^H is a tree. Again, hatched disks indicate almost overlapping placement of disks. Necessary infinitesimal bends are omitted. The direction of these bends of the inner components is indicated with the grey arrow. The approximated regular hexagon is indicated by the dashed green outline.



(b) In the narrowest position, the UDR of a T_k^H can – similar to the rhombus – fold all inner arms to one side (here to the lower side), and theoretically, there is space to fold the outer arms inward as depicted. The UDR of the arms are however again pairwise overlap free and the largest reachable distance any point on the boundary of the union of disks can have from the approximated regular hexagon is $2\sqrt{3} + 1$. Note further that the folding of the rightmost arm is not possible as depicted, indicated by the red crossings, which mark areas of forced overlap. However in a setting with an extremely long arm, the small inward bend could lead to almost parallel arms, which run very close to each other, hence we analyze the (unreachable) worst case.

4 Recognition Algorithm for Caterpillars

We propose a linear-time algorithm using similar ideas to Klemz et al. [13], that recognizes if an input caterpillar graph $G = (V, E)$ admits a UDR or not, and provides the representation if one exists. However, we need to address several issues as a larger class of graphs admits a UDR compared to a UDC. Note, the input graph $G = (V, E)$ is essentially a tree whose internal nodes form a backbone path $B_P = \{v_1, \dots, v_k\}$ for some $k \in \mathbb{N}$. Observe that, if G contains a vertex of degree 6, then due to the disk packing property, it does not admit a UDR. Therefore, we know that every realizable caterpillar must have the maximum degree $\Delta \leq 5$. Moreover, it is easy to observe that all caterpillars with $\Delta \leq 4$ admit a UDC (and thus a UDR), as also noted by Klemz et al. [13]. However, not every caterpillar with $\Delta = 5$ is realizable as UDR. We show that two consecutive degree-5 vertices on B_P cannot be realized.

4.1 The Algorithm

The following lemma characterizes a “No” instance for the algorithm presented in Section 4.

► **Lemma 4.1.** *If B_P contains two adjacent degree 5 vertices u, v , then it does not admit a unit disk intersection representation.*

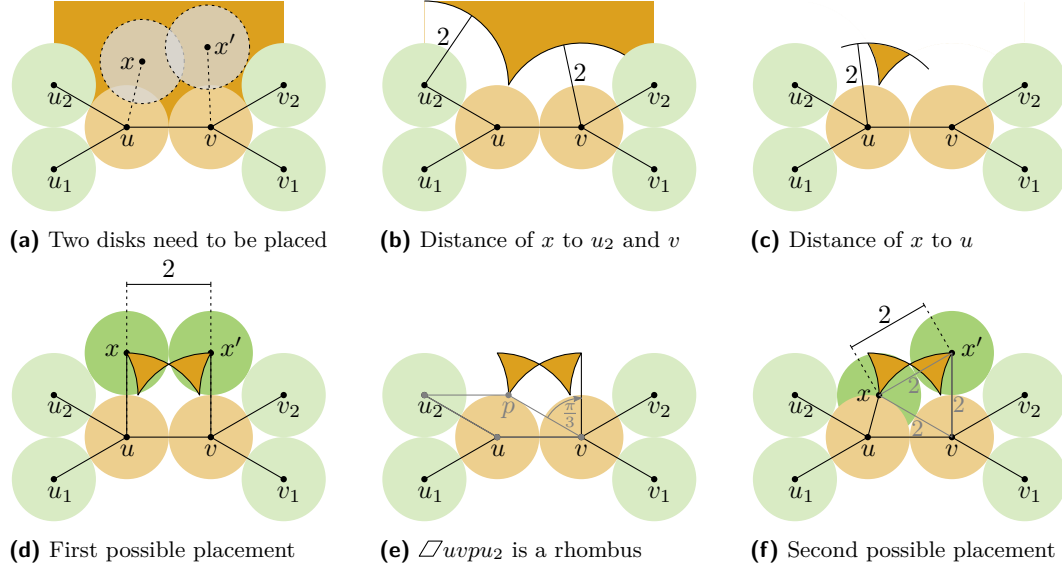
Proof. Let u_1, u_2, x (resp. v_1, v_2, x') be the first, second and third neighbor of u (resp. v) in counterclockwise/clockwise order, respectively. We assume a placement of $d(u_1), d(u_2), d(v_1)$ and $d(v_2)$ as depicted in Figure 11. Since x is adjacent to u and not adjacent to u_2 and v , the possible space of placing the center of $d(x)$ is restricted to a small open fan-shaped area (see Figure 11c). A symmetric area exists for $d(x')$ as well. Moreover, all three pairs of points with a distance of at least two, namely Figures 11d and 11f and a symmetric version of Figure 11f, are on the boundaries of these areas. Therefore no such pair exists in the open fan-shaped areas. Note that a similar argument holds for the lower side and any rotation of $d(u_1), d(u_2), d(v_1)$ or $d(v_2)$ will decrease the area on one side. This completes the proof. ◀

As a preprocessing step we augment all spine vertices of degree 3 or lower with additional degree 1 neighbors, s. t., they have degree 4. Consider a chain of vertices of degree 4 or lower. We place them on a horizontal line. At each disk $d(v_k)$, we place its leaf neighbor disks $d(v_k^t), d(v_k^b)$ first at the top and then at the bottom of $d(v_k)$, see Figure 12a, s. t., the clockwise angle $\angle v_k^t v_k v_k^b = \frac{4\pi}{3} - 2k\varepsilon$. The rotational ε offset avoids adjacencies between the leaf disks. While these offsets can add up, we can choose ε small enough for every finite caterpillar, s. t., this is negligible.

When we encounter a degree 5 vertex u after a degree four vertex v_k , we place the disk of its additional leaf $u^{t'}$ on the top side with a $\frac{\pi}{3} + \varepsilon$ rotational offset to $d(u^t)$, and therefore $\angle u^{t'} u u^b \leq \pi - (2k + 1)\varepsilon$, i. e., an almost horizontal connection, see Figure 12b.

If the next vertex x has also degree five, then due to Lemma 4.1 we know that the sequence is not realizable. Otherwise, we place $d(x)$, s. t., it is touching $d(u)$ with a $\frac{\pi}{3} + \varepsilon$ rotational offset to $d(x)$, see Figure 12b. We place $d(x^b)$ at the planned position relative to $d(x)$ at the bottom, i. e., with a $\frac{\pi}{3} + (k + 2)\varepsilon$ counter clockwise offset relative to the x -axis, however, we place $d(x^t)$ almost exactly on top of $d(x)$ with a very small shift of $\frac{\varepsilon}{C_n}$ orthogonal to \overline{ux} , for some large constant C . This prevents touching of $d(u)$ and $d(x^t)$, without creating an adjacency between $d(u^{t'})$ and $d(x^t)$.

From this point onwards, we consider the direction of \overline{ux} to be the direction in which we extend the spine of the caterpillar. Any following disk $d(v_{k+3})$ can be placed again in the new extension direction touching $d(x)$. Its leaf disks $d(v_{k+3}^t)$ and $d(v_{k+3}^b)$ can be placed



■ **Figure 11** Visualization of the proof steps of Lemma 4.1. The area highlighted in orange illustrates possible placements for the center of $d(x)$, which is progressively restricted by its adjacent and non-adjacent neighbors.

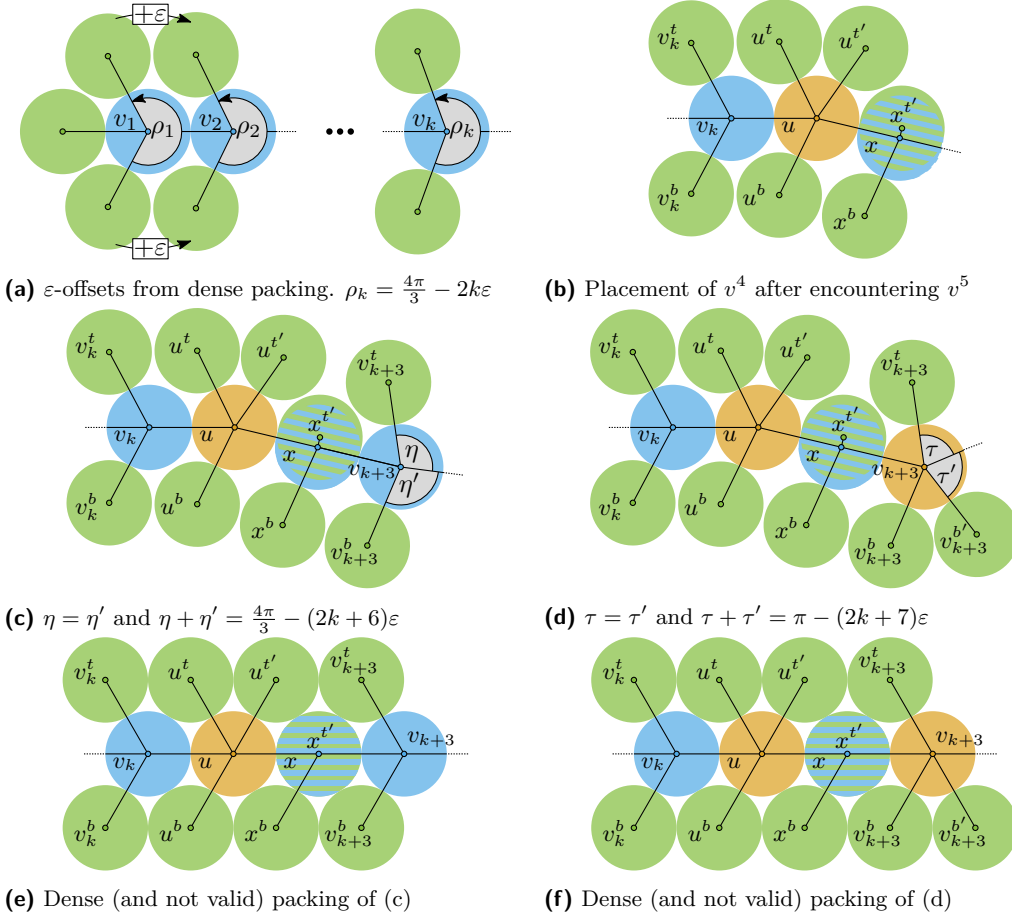
in their planned positions, i.e. with a clockwise or counterclockwise offset of $\frac{\pi}{3} + (k+3)\varepsilon$ relative to the new extension direction, respectively, which results in a clockwise angle $\angle u_t u u_b \leq \frac{4\pi}{3} - (2k+6)\varepsilon$. Note that v_{k+3} can have a degree of four or lower (Figure 12c) or five (Figure 12d). Note that at this point, if v_{k+3} has degree 5, we can immediately repeat this procedure.

As a final postprocessing step, we remove all degree 1 vertices that are added in the preprocessing step. At the first encountered vertex of degree 5, we place its third leaf neighbor ($d(u^t)$ in the previous paragraphs) at the top. Then we place the third leaf neighbor of a spine vertex of degree 5, alternatingly twice at the bottom and twice at the top. This returns new extension direction to being horizontal after every second spine vertex of degree 5. In between it has alternatingly only a slight positive or negative angle offset relative to the x -axis.

Note that, the rotational offset angles in Figure 12 are exaggerated, for better readability. The versions without (or with infinitesimal) rotational offset are depicted in Figures 12e and 12f.

Correctness. If a caterpillar contains consecutive degree 5 vertices we reject it as it has no UDR. In any other case, the algorithm above can represent it in a way, s.t., at any point the angle between a spine vertex and its left most-top and left-most bottom leaf is less than π . As long as this property holds, we can always add a new spine vertex. Moreover, if the sequence is extended by a spine vertex of at most degree 4, this property immediately holds again. If the sequence is extended by a spine vertex of degree 5, a spine vertex of degree at most 4 must follow. Once we place this degree 4 vertex appropriately, cf. Figure 12b, then the property immediately holds again.

From the above description of the algorithm and the correctness analysis we conclude the following theorem.



■ **Figure 12** Chains of degree 4 are placed in a dense packing formation with small offsets (a). A degree five vertex places an additional leaf on one side (b). The following vertex of degree at most 4 places its leaf on the same side almost on top of itself. The next vertex x can again be placed with the desired angle of just over $\frac{2\pi}{3}$ between two neighbors. Placement of x is possible if its degree 4 (c) or 5 (d). The (not valid) dense packing versions of (b)/(c) can be seen in (e)/(f).

► **Theorem 4.2.** *Given a caterpillar graph $G = (V, E)$, it can be decided in linear time whether G is a unit disk graph. Moreover, if an unit disk intersection representation exists then it can be constructed in linear time.*

From Lemma 4.1 and Theorem 4.2, we get the following corollary.

► **Corollary 4.3.** *Let $G = (V, E)$ be a caterpillar graph. G admits a unit disk intersection representation if and only if G does not contain any two adjacent degree 5 vertices in the backbone path B_P of G .*

5 Acknowledgement

The authors want to thank Maarten Löffler, Jonas Cleve, and Man-Kwun Chiu for fruitful discussions about the project during their research visits in Vienna.

References

- 1 Clinton Bowen, Stephane Durocher, Maarten Löffler, Anika Rounds, André Schulz, and Csaba D. Tóth. Realization of simply connected polygonal linkages and recognition of unit disk contact trees. In *Graph Drawing and Network Visualization (GD'15)*, volume 9411 of *LNCS*, pages 447–459. Springer International Publishing, 2015. doi:[10.1007/978-3-319-27261-0_37](https://doi.org/10.1007/978-3-319-27261-0_37).
- 2 Heinz Breu and David G. Kirkpatrick. On the complexity of recognizing intersection and touching graphs of disks. In Franz J. Brandenburg, editor, *Graph Drawing (GD'95)*, volume 1027 of *LNCS*, pages 88–98. Springer, 1996. doi:[10.1007/BFb0021793](https://doi.org/10.1007/BFb0021793).
- 3 Heinz Breu and David G. Kirkpatrick. Unit disk graph recognition is NP-hard. *Comput. Geom. Theory Appl.*, 9(1–2):3–24, 1998. doi:[10.1016/S0925-7721\(97\)00014-X](https://doi.org/10.1016/S0925-7721(97)00014-X).
- 4 Jérémie Chalopin, Daniel Gonçalves, and Pascal Ochem. Planar graphs have 1-string representations. *Discrete & Computational Geometry*, 43(3):626–647, 2010. doi:[10.1007/s00454-009-9196-9](https://doi.org/10.1007/s00454-009-9196-9).
- 5 Steven Chaplick and Torsten Ueckerdt. Planar graphs as VPG-graphs. In Walter Didimo and Maurizio Patrignani, editors, *Graph Drawing (GD'12)*, volume 7704 of *LNCS*, pages 174–186. Springer, 2013. doi:[10.1007/978-3-642-36763-2_16](https://doi.org/10.1007/978-3-642-36763-2_16).
- 6 Man-Kwun Chiu, Jonas Cleve, and Martin Nöllenburg. Recognizing embedded caterpillars with weak unit disk contact representations is NP-hard. *CoRR*, abs/2010.01881, 2020. arXiv:[2010.01881](https://arxiv.org/abs/2010.01881).
- 7 Jonas Cleve. Weak unit disk contact representations for graphs without embedding. *CoRR*, abs/2010.01886, 2020. arXiv:[2010.01886](https://arxiv.org/abs/2010.01886).
- 8 Peter Eades and Nicholas C. Wormald. Fixed edge-length graph drawing is np-hard. *Discrete Applied Mathematics*, 28(2):111–134, 1990. doi:[10.1016/0166-218X\(90\)90110-X](https://doi.org/10.1016/0166-218X(90)90110-X).
- 9 Stefan Felsner. Rectangle and square representations of planar graphs. In János Pach, editor, *Thirty Essays on Geometric Graph Theory*, pages 213–248. Springer, 2013. doi:[10.1007/978-1-4614-0110-0_12](https://doi.org/10.1007/978-1-4614-0110-0_12).
- 10 Daniel Gonçalves, Lucas Isenmann, and Claire Pennarun. Planar graphs as L-intersection or L-contact graphs. In *Discrete Algorithms (SODA'18)*, pages 172–184. SIAM, 2018. doi:[10.1137/1.9781611975031.12](https://doi.org/10.1137/1.9781611975031.12).
- 11 Petr Hliněný. Classes and recognition of curve contact graphs. *Journal of Combinatorial Theory, Series B*, 74(1):87–103, 1998. doi:[10.1006/jctb.1998.1846](https://doi.org/10.1006/jctb.1998.1846).
- 12 Petr Hliněný and Jan Kratochvíl. Representing graphs by disks and balls (a survey of recognition-complexity results). *Discrete Mathematics*, 229(1):101–124, 2001. doi:[10.1016/S0012-365X\(00\)00204-1](https://doi.org/10.1016/S0012-365X(00)00204-1).
- 13 Boris Klemz, Martin Nöllenburg, and Roman Prutkin. Recognizing weighted disk contact graphs. In *Graph Drawing and Network Visualization (GD'15)*, volume 9411 of *LNCS*, pages 433–446. Springer International Publishing, 2015. doi:[10.1007/978-3-319-27261-0_36](https://doi.org/10.1007/978-3-319-27261-0_36).
- 14 Paul Koebe. Kontaktprobleme der konformen Abbildung. *Ber. Sächs. Akad. Wiss. Leipzig, Math.-Phys. Klasse*, 88:141–164, 1936.